OAK RIDGE NATIONAL LABORATORY
operated by
UNION CARBIDE CORPORATION
for the
U.S. ATOMIC ENERGY COMMISSION

ORNL-TM-552

COPY NO. - 53

DATE - May 21, 1963

MATERIAL REQUIREMENTS FOR SHIELDING AGAINST SPACE RADIATIONS*

Clayton D. Zerby

Abstract

A brief but general discussion of the material requirements for shielding against space radiations is presented. Emphasis is placed on describing the salient features of the space radiation attenuation problem in order to deduce the materials that will most likely produce minimum-weight shields. The shielding characteristics of the materials are described as a function of atomic weights and no specific materials are referred to. In general it is found that the light atomic weight elements give the minimum-weight shields.

*Paper presented at the American Nuclear Society Meeting (Southwestern Ohio Section), Cincinnati, Ohio, April 17-19, 1963.

NOTICE

This document contains information of a preliminary nature and was prepared primarily for internal use at the Oak Ridge National Laboratory. It is subject to revision or correction and therefore does not represent a final report. The information is not to be abstracted, reprinted or otherwise given public dissemination without the approval of the ORNL patent branch, Legal and Information Control Department.

LEGAL NOTICE

This report was prepared as an account of Government sponsored work. Neither the United States, nor the Commission, nor any person acting on behalf of the Commission:

A. Makes any warranty or representation, expressed or implied, with respect to the accuracy, completeness, or usefulness of the information contained in this report, or that the use of any information, apparatus, method, or process disclosed in this report may not infringe privately owned rights; or

B. Assumes any liabilities with respect to the use of, or for damages resulting from the use of any information, apparatus, method, or process disclosed in this report.

As used in the above, "person acting on behalf of the Commission" includes any employee or contractor of the Commission, or employee of such contractor, to the extent that such employee or contractor of the Commission, or employee of such contractor prepares, disseminates, or provides access to, any information pursuant to his employment or contract with the Commission, or his employment with such contractor.

The purpose of this report is to present a quite brief but general discussion of the material requirements for shielding against space radiations. Although a brief review of the sources of radiation is presented first, the major emphasis is placed on describing the salient features of the radiation penetration problem with the intent of deducing the materials that will most likely yield minimum-weight shields. This is done in the broadest sense by indicating trends in terms of atomic weights of the materials and no specific materials are referred to.

No attempt has been made to estimate shield weights required for various missions because this requires discussions of topics beyond the intended scope of the present paper. To include such estimates would require discussion of the possible mission trajectory and a discussion of the maximum permissible dose from the penetrating radiation that could be allowed. These subjects would obviously lead us too far afield.

Sources of Radiation

Turning to the sources of radiation, it should be noted that the space radiations that are likely to constitute a radiation hazard are all charged particles. This is true in general because only charged particles can be trapped in a planet's magnetic fields and build up to high intensities or can be accelerated to high energies in the varying magnetic fields in space. Photon intensities in space appear to be very small and of little concern. Neutral particle intensities also appear to be very small since these particles are not accelerated by electric or magnetic forces and generally decay into charged particles within a short distance of their creation because of their relatively short half lives.

Van Allen has recently summarized the locations and intensities of the geomagnetically trapped radiation found in the two natural radiation belts.[1] Figures 1 through 3 are reproductions of his data. Figure 1 shows the location of the inner radiation belt, which is centered about 1400

---

1. J. A. Van Allen, "Brief Note on the Radiation Belts of the Earth," Paper A-1, Proceedings of the Symposium on the Protection Against Radiation Hazards in Space, TID-7652 (1963).

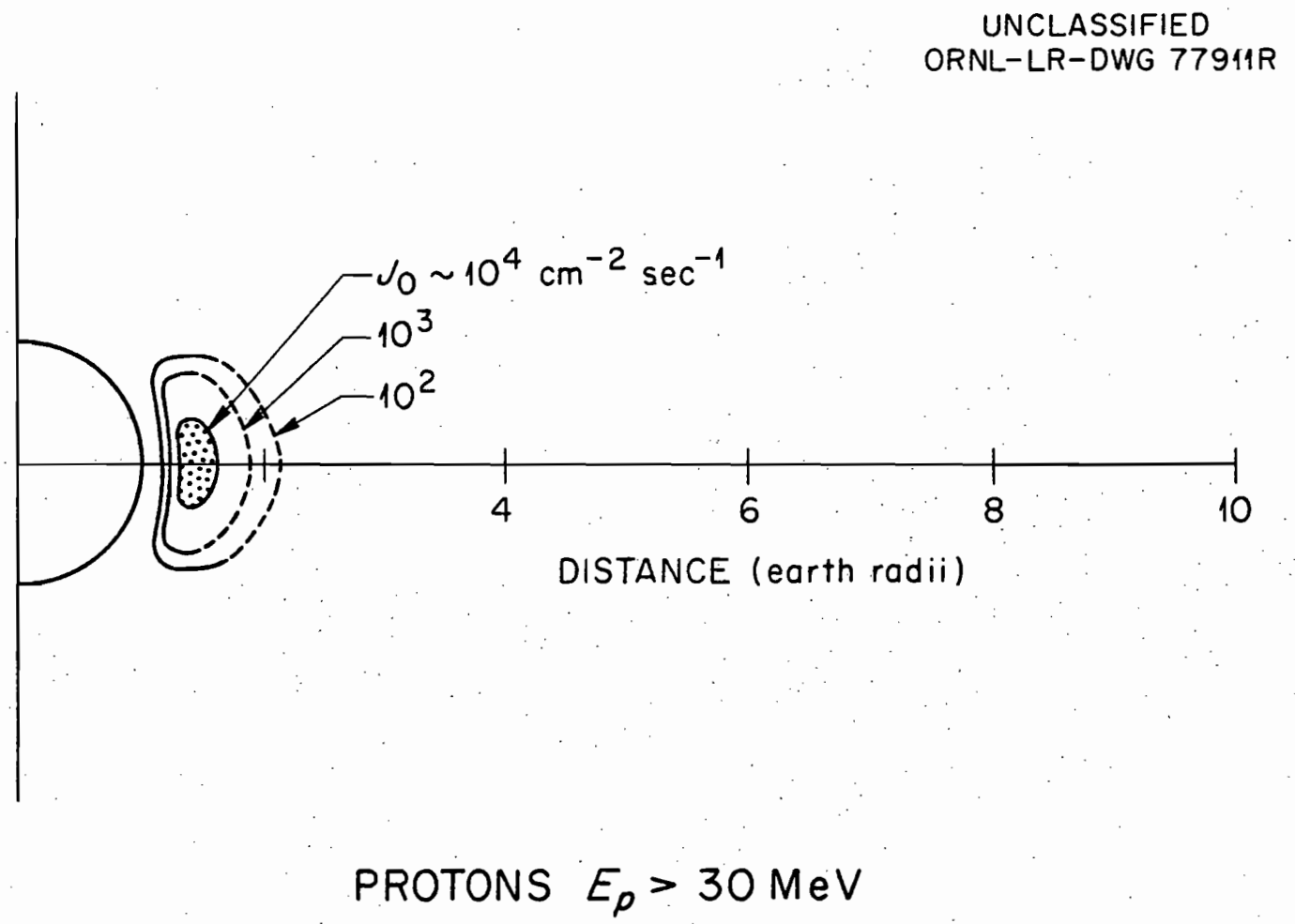

Fig. 1. Omnidirectional Flux of Protons Above 30 MeV in the Inner Radiation Belt.

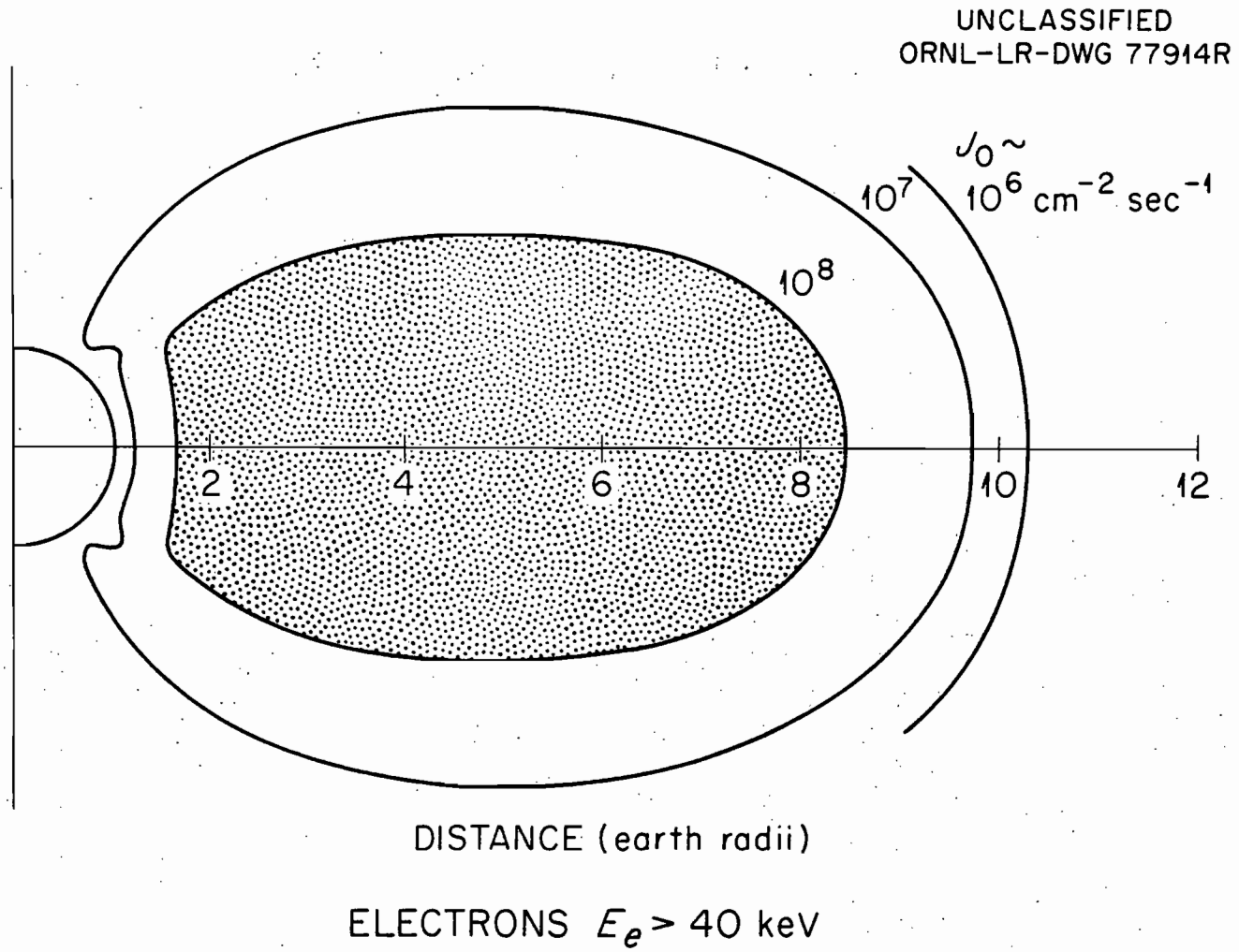

Fig. 2. Omnidirectional Flux of Electrons Above 40 KeV in the Outer Radiation Belt.

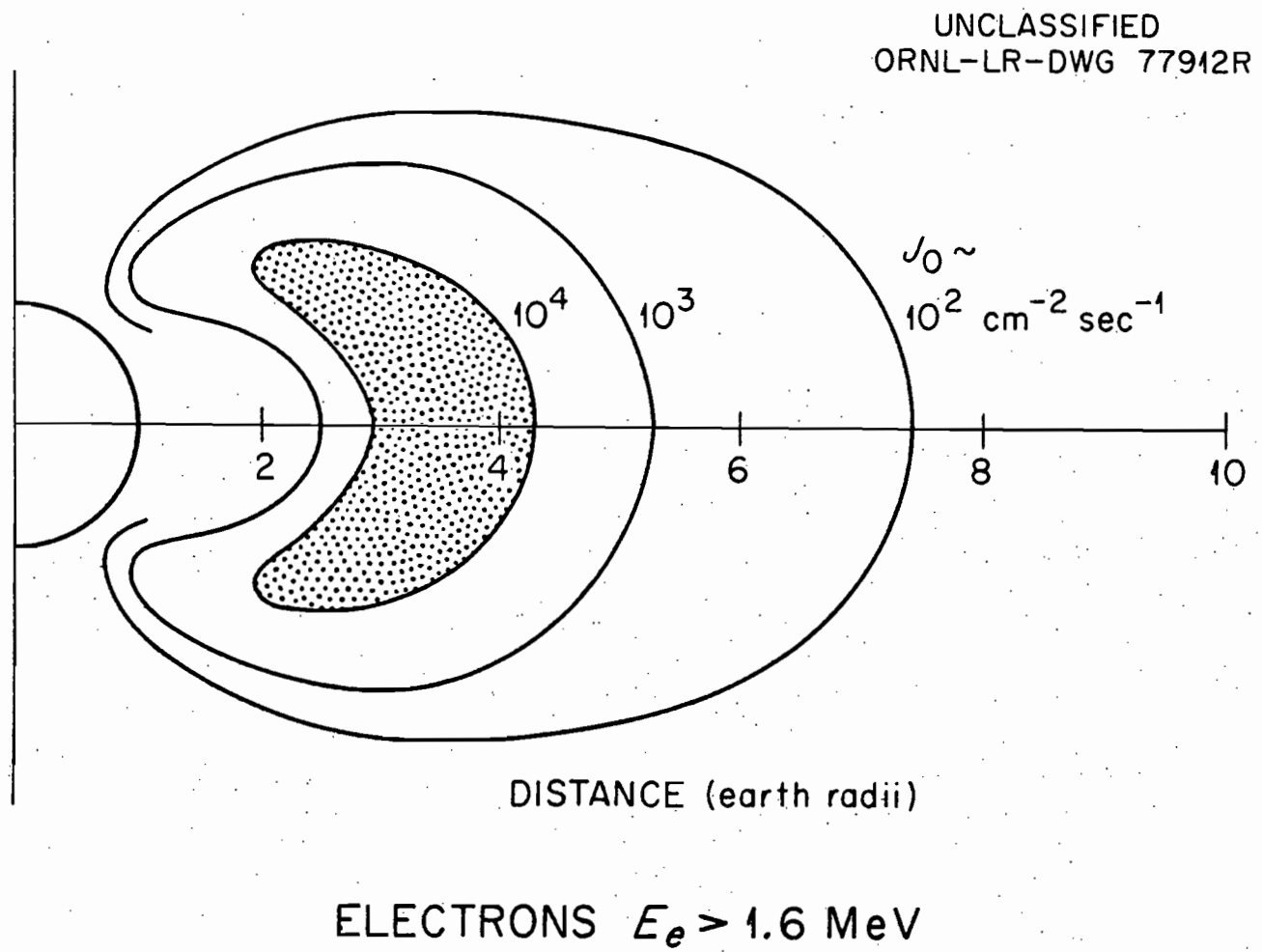

Fig. 3. Omnidirectional Flux of Electrons Above 1.6 MeV in the Outer Radiation Belt.

miles above the earth's surface on the geomagnetic equator. This belt is very stable and consists mainly of high-energy protons ranging in energy to approximately 700 MeV. The outer radiation belt consists of electrons with energies up to 5 or 6 MeV and of low-energy protons. Figure 2 indicates the omnidirectional flux of the electrons above 40 kev, and Fig. 3 shows the omnidirectional flux of electrons greater than 1.6 MeV. It should be noted that the highest intensity of high-energy electrons is centered between 3 and 4 radii from the center of the earth. The intensities shown in Fig. 3 are typical of those that might be encountered during periods of inactivity on the sun.

Figure 4 presents the integral and differential spectrum of the electrons in the heart of the outer radiation belt. The data points are those of O'Brein et al.[2] It will be noticed that the differential spectrum falls off steeply with energy and becomes negligible at 5 or 6 MeV.

The location of the low-energy protons in the outer belt is approximately represented by that shown for the electrons in Fig. 2. Although these protons have flux values as high as 10^8 particles/cm^2-sec, their maximum energy is only 5 MeV; therefore they can be neglected as a radiation hazard because they can be stopped by a shielding material a few tenths of a g/cm^2 thick.

Deviating slightly from the discussion of natural radiation belts, it is appropriate to call attention to the artificial belt created by the July 9, 1962, high-altitude nuclear detonation. A high flux of electrons from the beta decay of fission products from the blast was trapped in the geomagnetic field at altitudes above approximately 200 miles. The flux of electrons reached values as high as 10^9 particles/cm^2-sec immediately after the blast, and is still persisting at high flux values at this time. The energy of these particles has ranged up to 7 or 8 MeV.

The spectrum of electrons that is expected to be present in the artificial radiation belt is shown in Fig. 5. The curve was taken from the beta-decay spectrum from fission fragments reported by Carter et al.[3]

2. B. J. O'Brein et al., J. Geophys. Res. 67, 397 (1962).
3. C. E. Carter, F. Reines, J. J. Wagner, and M. E. Wyman, Phys. Rev. 113, 280 (1959).

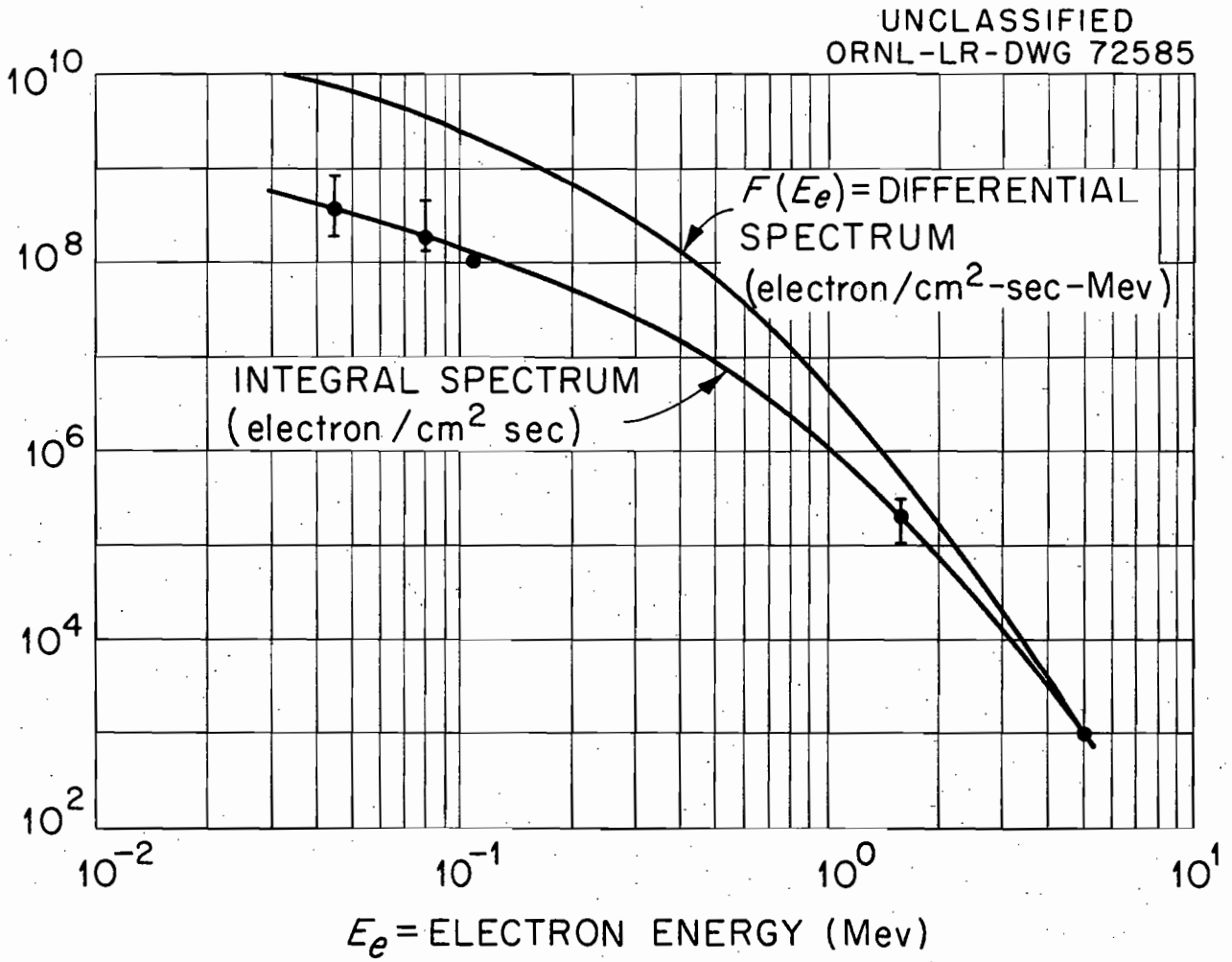

Fig. 4. Omnidirectional Flux of Electrons in the Heart of the Outer Radiation Belt. Based on the experiment of B. J. O'Brein et al. [J. Geophys. Res. 67, 397 (1962)].

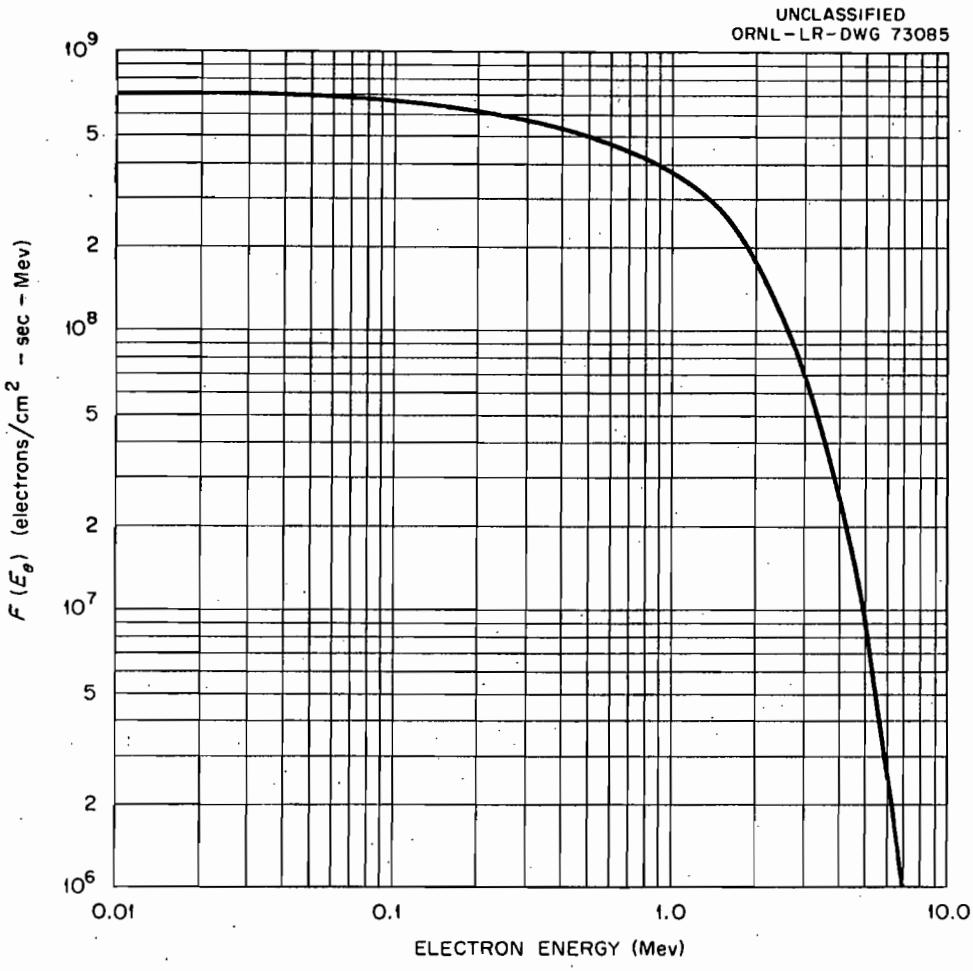

Fig. 5. Maximum Omnidirectional Flux of Electrons in the Earth's Artificial Radiation Belt.

and was normalized to a total of 10^9 particles/cm^2-sec to represent the intensity of radiation that was present immediately after the nuclear blast. This spectrum is significantly different from that existing in the outer Van Allen radiation belt in that it is much flatter below 1 MeV. Above that energy, however, it drops off steeply, becoming negligible at 6 or 7 MeV.

Turning briefly to cosmic rays, it is appropriate to note that the sun is a source of high-energy protons. Frequently, active regions are created on the sun which emit high fluxes of protons ranging in energy up to 10 Bev. In most cases, however, the intensity is sufficiently low at 1 Bev for us to say that this is effectively the upper energy bound for solar protons. Figure 6 shows some typical integral spectra of solar protons.[4] The spectrum of the protons in the inner radiation belt and the primary protons of galactic origin that arrive from space are also shown in Fig. 6 for comparison purposes. The galactic protons will range in energy into the hundreds of Bev. However, the intensity is sufficiently low that this source of radiation is not likely to constitute a radiation hazard.

To summarize the information on the sources of radiation, there are high-energy protons ranging up to 700 MeV in the inner Van Allen belt centered at 1400 miles above the earth's surface, and high-energy protons coming from solar-active regions. The energy of the solar protons can at times be as high as 1 Bev and, infrequently, as high as 10 Bev. Galactic cosmic rays have energies ranging up into the hundreds of Bev, but with sufficiently low intensity to be of little concern. Electrons occur naturally in the outer Van Allen belt with energies up to 5 or 6 MeV and also persist in the artificial belt with energies up to 6 or 7 MeV.

Shielding Against Space Radiations

In the matter of shielding against the radiations described above, the electron attenuation problem will be considered first. For electrons with energies below 10 MeV the major mechanism of energy degradation is

---

4. Trutz Foelsche, Current Estimates of Radiation Doses in Space, NASA TN D-1267 (July 1962).

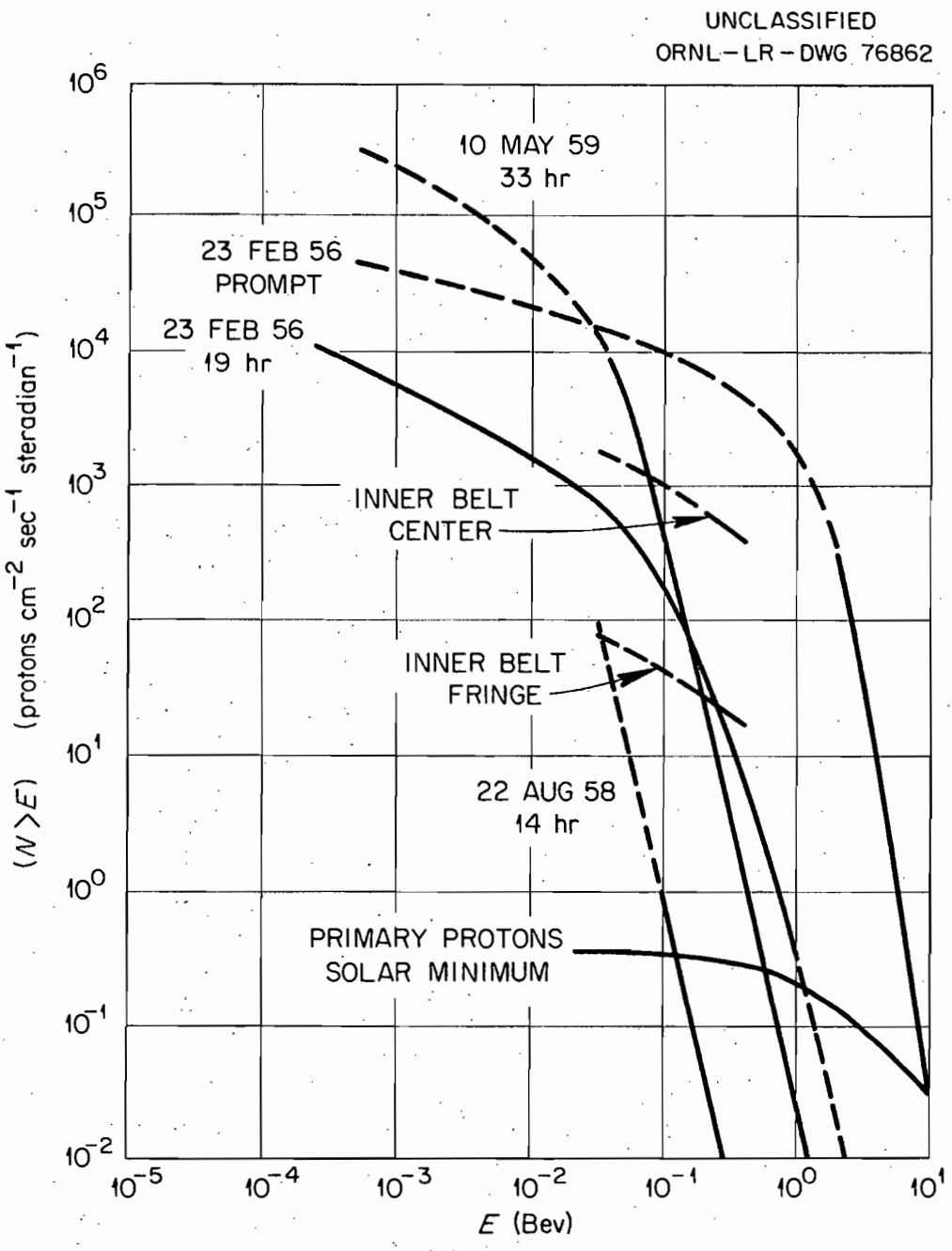

Fig. 6. Omnidirectional Flux of Protons from Solar Flares and Other Natural Sources.

collisions with atomic electrons. These collisions are so frequent that the process can be treated as a continuous one, and the average energy loss per unit path length traveled, called the "stopping power," can be calculated. The stopping power of several materials for electrons is presented in Fig. 7 in units of MeV/g-cm^{-2}, which yields a comparison of the effectiveness of materials on a weight basis, the material of the higher curve giving the greatest energy removal for the least weight. Thus we see that the light-atomic-weight elements appear to be the best materials for stopping electrons. This fact is demonstrated in another way in Fig. 8, which shows the maximum range in g/cm^2 that electrons will travel in a given material.

A very rough approximation to the range-energy curves is that the residual range in g/cm^2 is equal to the incident energy expressed in MeV. Thus a 10-MeV electron will be stopped by approximately 10 g/cm^2 of material and a 1-MeV electron will be stopped by approximately 1 g/cm^2 of material. It is therefore clear that it will take approximately 5 to 7 g/cm^2 of material to stop all the electrons that might be encountered in the artificial belt and the outer Van Allen radiation belt.

The electron shielding problem would be relatively simple if collisions with atomic electrons were the only interactions that could take place as electrons pass through the material. However, occasionally the electron will make a radiative collision in the process of diffusing through the material and give rise to bremsstrahlung radiation. The spectra of the bremsstrahlung emitted for electrons slowing down in the charring ablator of a capsule are shown in Fig. 9.[5] Of special significance is the steepness of the spectra, which indicates an abundance of low-energy photons produced in radiative collisions. Although the yield of bremsstrahlung is relatively small for electrons slowing down in the ablator material, when it is multiplied by the high flux of electrons a significant number of photons results. For example, if a 3-g/cm^2-thick shield with an outer layer of ablator is exposed to the electrons in the

---

5. Neutron Phys. Div. Space Radiation Shielding Res. Ann. Prog. Rep. Aug. 31, 1962, ORNL-CF-62-10-29 (Rev.) (1962), Paper I-11, Fig. 2.

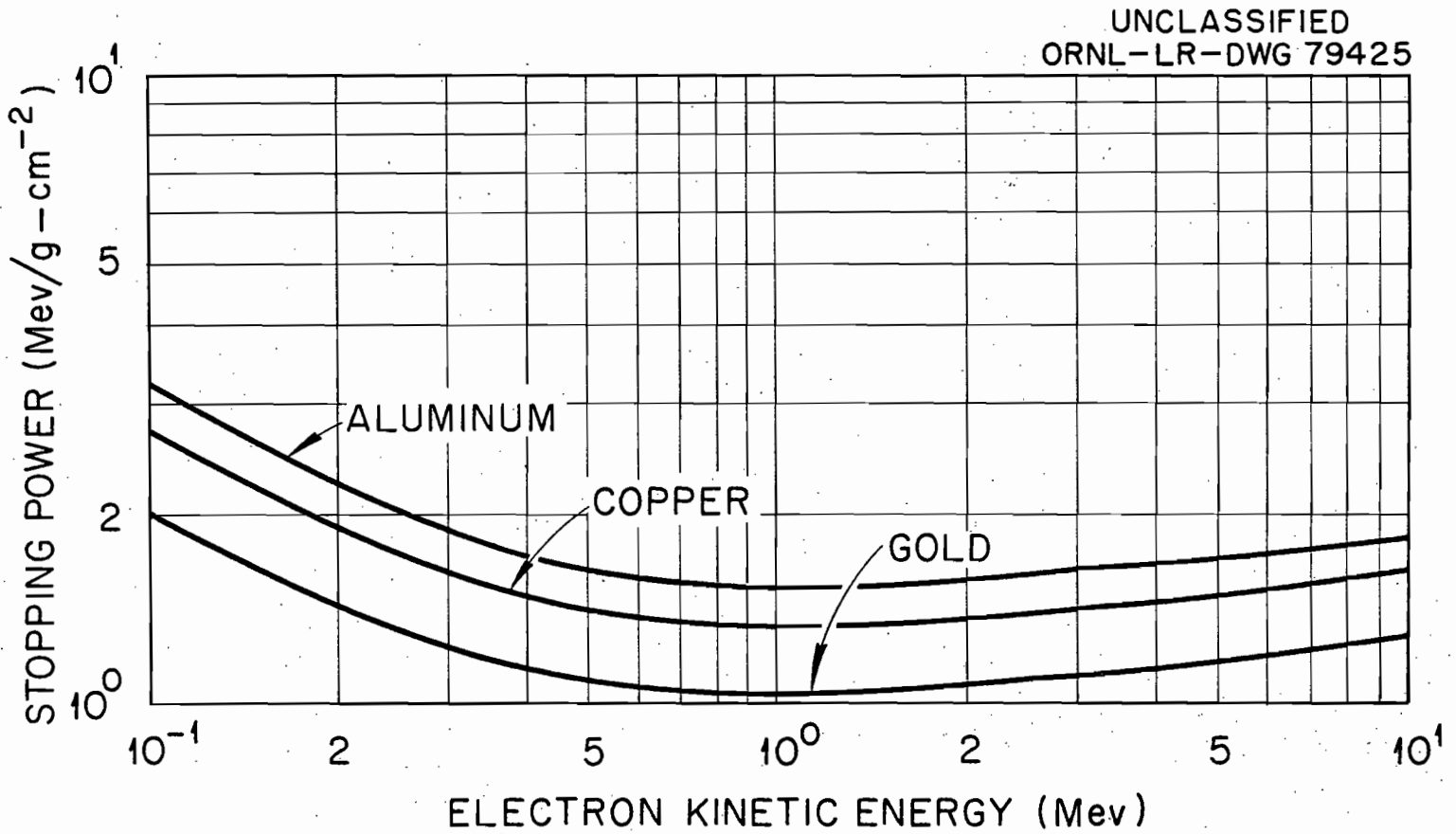

Fig. 7. Stopping Power for Electrons.

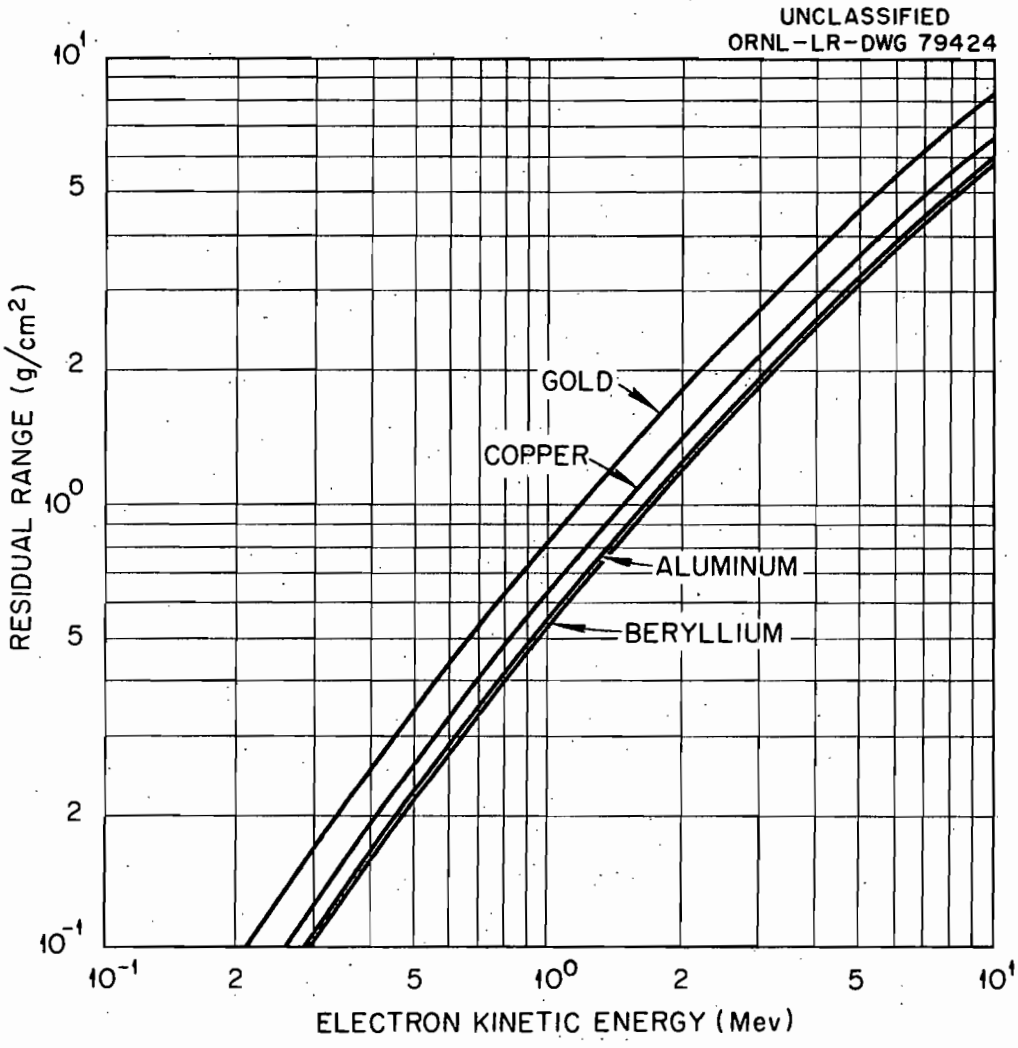

Fig. 8. Calculated Residual Range of Electrons.

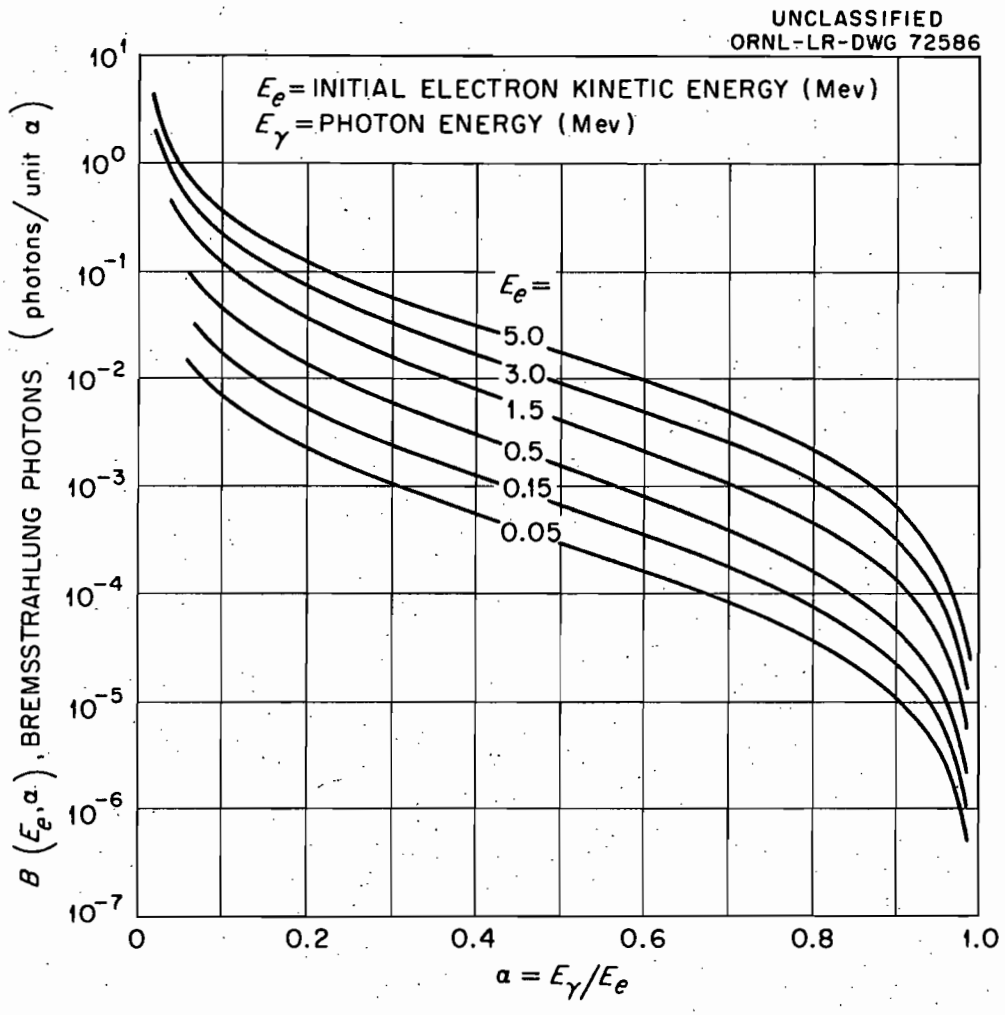

Fig. 9. Bremsstrahlung Radiation Produced in the Charring Ablator of an Apollo Vehicle.

heart of the artificial belt shortly after detonation, the dose behind the shield would be approximately 2 rads/hr from bremsstrahlung. This dose would be in addition to the dose from the penetrating electrons.

To minimize the production of bremsstrahlung, one would select a material with a low atomic charge since the cross section for bremsstrahlung is approximately proportional to the atomic charge squared. This means that a low-atomic-weight material not only produces a minimum-weight shield for stopping the electrons but also minimizes the production of secondary bremsstrahlung radiation. If a shield thicker than the range of the incident electrons is required in order to attenuate secondary bremsstrahlung, it would be best to use a thin inner layer of high-atomic-weight materials, since the photoelectric cross section which is so effective for stopping low-energy photons is proportional to the atomic charge to the fifth power.

In considering the problem of shielding against protons, we find that the major mechanism for stopping protons is also collisions with atomic electrons, and, as shown in Fig. 10, the light-atomic-weight materials again furnish the lightest weight shields. It should be noted in Fig. 10 that the low-energy protons are preferentially stopped by ionization collisions, which has a significant effect on the shape of a proton spectrum that is attenuated by a material, as is discussed below.

In Fig. 11 the residual range of the protons is presented as a function of the proton energy. From this figure it should be obvious that the more energetic particles that might be encountered in space will always penetrate the shielding material of a typical vehicle. As an example, consider the range of a 1-Bev proton in hydrogen, which is the most economical shielding material. In this case the shield thickness must be approximately 170 g/cm^2 to stop the proton. However, a shield of this thickness is not likely to be carried on a typical space vehicle and therefore some protons will usually penetrate to the inside of the vehicle.

Figure 12 shows how a typical flare spectrum is attenuated by an

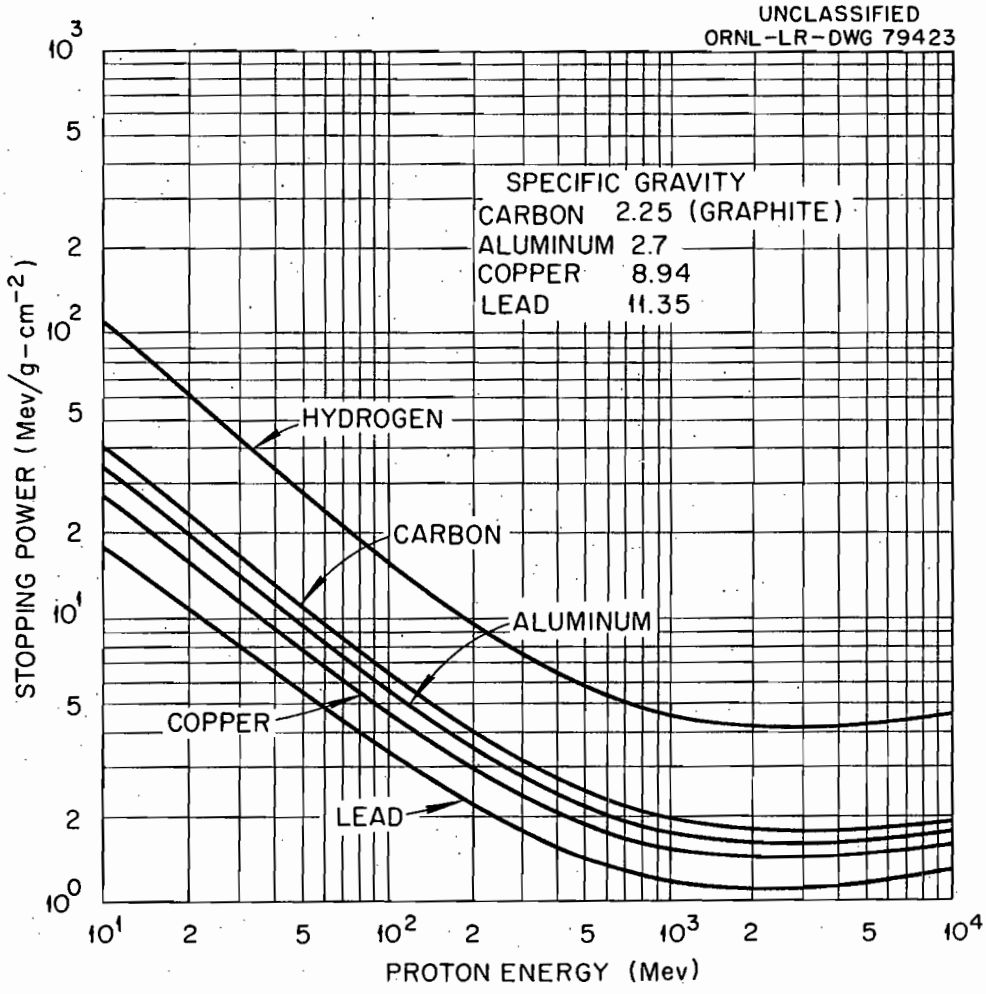

Fig. 10. Stopping Power for Protons.

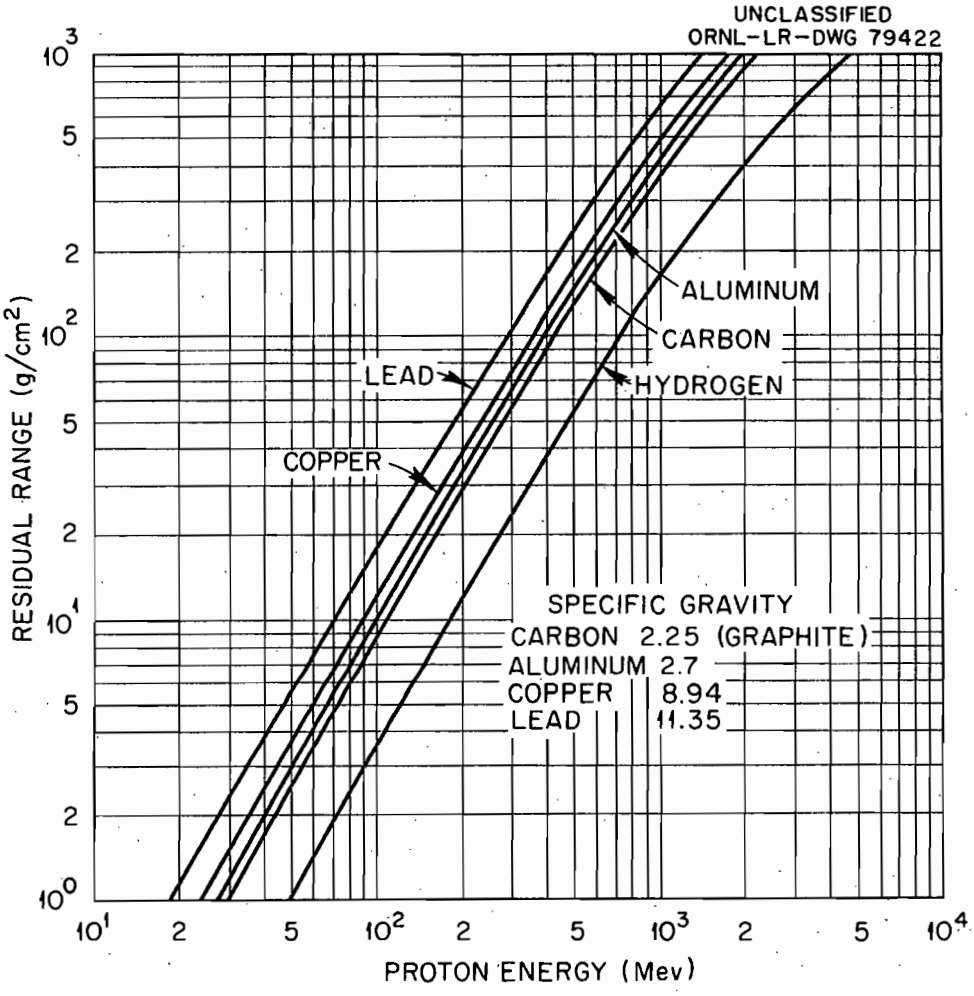

Fig. 11. Residual Range of Protons.

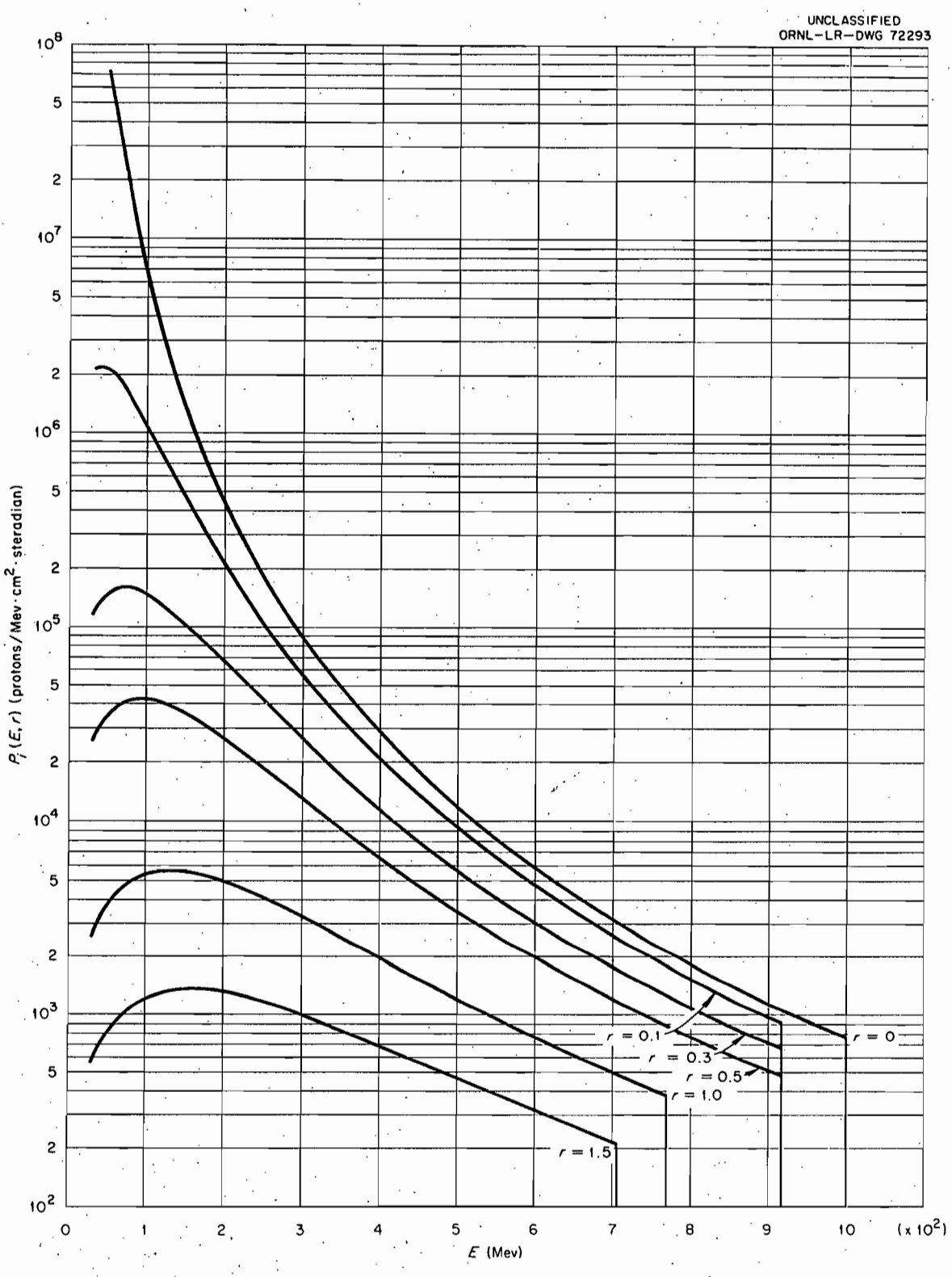

Fig. 12. Primary Proton Flux vs. Energy in Aluminum. Flare proton spectrum incident isotropically. r is measured in collision lengths (= 34.74 cm = 93.80 g/cm^2).

aluminum shield.[6] As the depth in the shield increases, the low-energy protons are preferentially removed by collisions with atomic electrons, and the curve tends to turn over and have a maximum. This also leads to a general hardening of the spectrum. By "hardening" is meant that the ratio of high-energy particles to low-energy particles tends to increase. Take, for example, the ratio of 600-MeV protons to 100-MeV protons. At zero depth the ratio is approximately 10^{-3}, but at a depth of $r = 1.5$, the ratio is 0.25.

As in the case of the attenuation of electrons, if collisions with the bound atomic electrons were the only interactions to be considered, the attenuation of the protons would be relatively simple. However, just as in the case of electrons, secondary radiation can be created, in this case by nonelastic interactions of the protons with the atomic nuclei. A schematic sketch of the interactions that are possible is shown in Fig. 13. The incident proton approaching from the left, ionizing atoms as it goes, can have a nuclear interaction and produce pions and other particles, as indicated in the upper part of the figure. For incident energies below 1 Bev, however, the particles ejected from the nucleus will be predominantly nucleons. These particles can, in turn, interact with other nuclei of the shielding material, as indicated in the lower part of Fig. 13.

A nucleus that has experienced a nonelastic event will usually be left in an excited state and boil off other nucleons, as well as give off gamma rays in the process of de-excitation. The boiled-off particles, especially the neutrons, then can have nonelastic scattering events or can be captured by other nuclei. The cross sections for high-energy nonelastic events for various elements in the periodic table[7,8] are shown in Fig. 14 (see also Table A-1 in Appendix A). They are essentially geometric but vary slightly with energy. The nonelastic cross section

---

6. R. G. Alsmiller, Jr. and J. E. Murphy, Space Vehicle Shielding Studies: Calculations of the Attenuation of a Model Solar Flare and Monoenergetic Proton Beams by Aluminum Shields, ORNL-3317 (1962), Fig. 4.
7. H. W. Bertini and L. Dresner, Neutron Phys. Div. Space Radiation Shielding Research Ann. Prog. Rep. Aug. 31, 1962, ORNL-CF-62-10-29 (Rev.) (1962), Paper I-2, p. 58.
8. Tables of data taken from the calculations of H. W. Bertini and L. Dresner referred to in Ref. 7 are included in the Appendix.

UNCLASSIFIED
ORNL-LR-DWG 77422

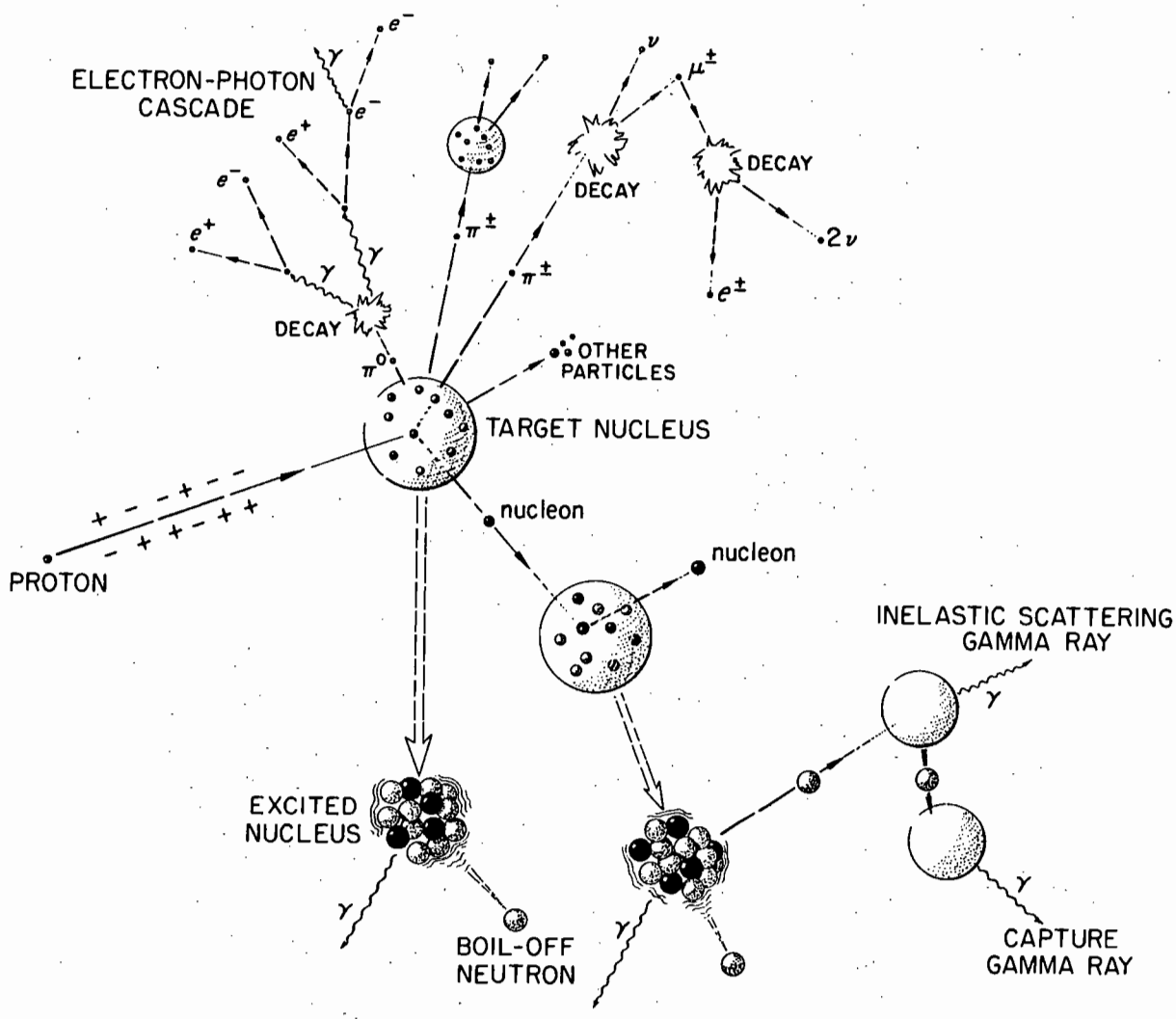

Fig. 13. Radiation Induced in Materials by High-Energy Protons.

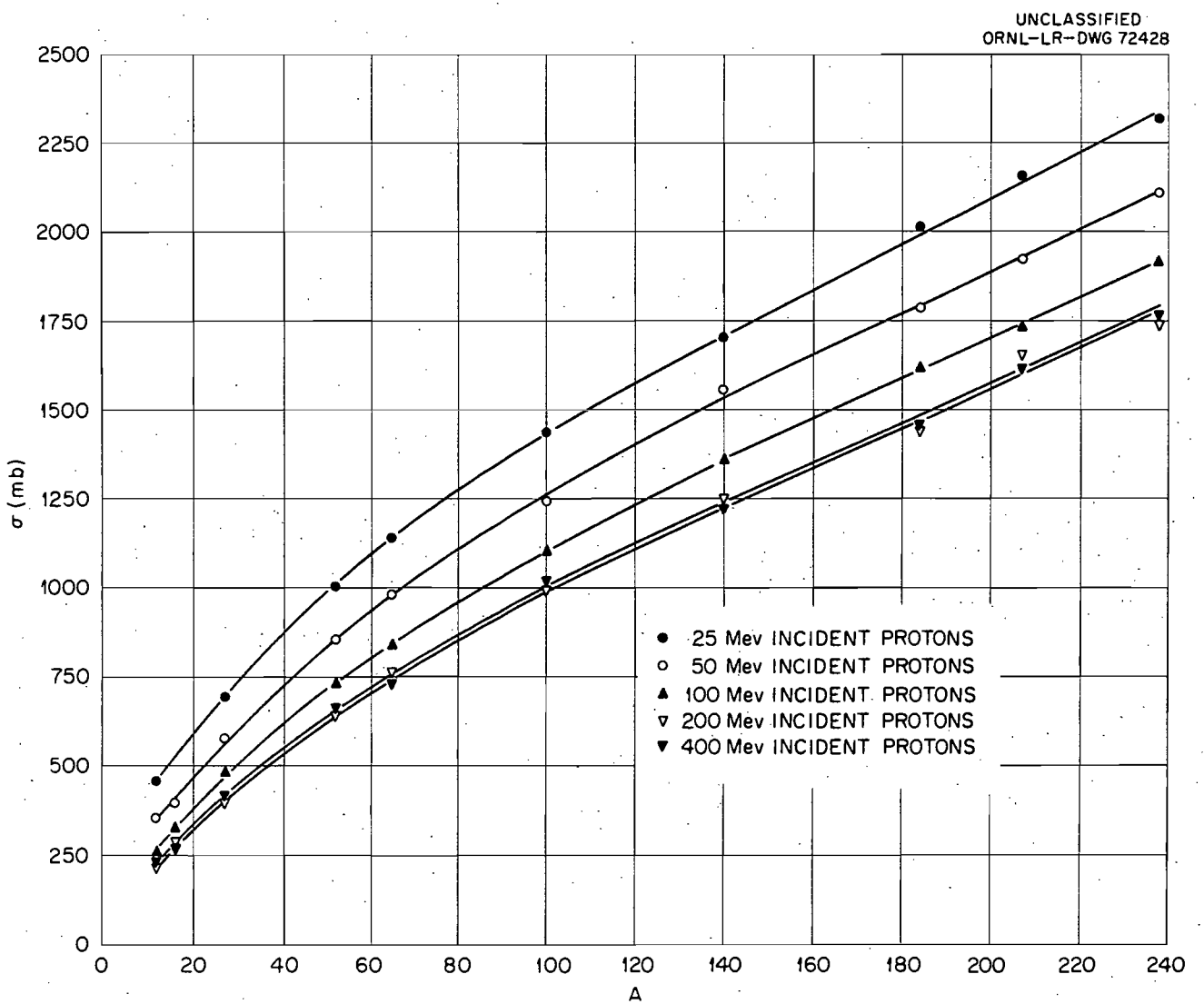

Fig. 14. Total Nonelastic Cross Section vs. Atomic Mass Number A for Incident Protons.

for light elements such as carbon is approximately 250 to 500 mb, whereas the cross section for the heavy elements such as uranium is approximately 2 barns.

The average number of cascade and evaporation neutrons emitted as a result of a nonelastic event between a proton and a nucleus is given in Fig. 15 as a function of the atomic mass number.[7,8] For 400-MeV incident protons the average number of neutrons increases linearly from approximately 1 for carbon to approximately 12 for a material such as uranium. The average number of cascade protons as a function of the atomic mass number[8] is shown in Fig. 16. Here, the average number for 400-MeV incident protons is approximately 1.5 over the whole periodic table. This information is given in tabular form in Appendix A, which also includes tables giving the average energy of the cascade and evaporation particles.

The significance of these nonelastic interactions in comparison with the collisions with the bound atomic electrons is indicated in Fig. 17. The dashed curves represent the energy deposited by ionization collisions and are the stopping-power curves of Fig. 10. The curves showing the energy removed by nonelastic interactions were obtained by multiplying the nonelastic cross section by the incident energy of the proton, since this correctly gives the energy removed from the primary beam. It will be noticed that the energy-removed curves cross the energy-deposited (dashed) curves at approximately 300 MeV for each material. This suggests again that the light-atomic-weight materials are the materials which yield the lightest-weight shields.

The curves in Fig. 17 labeled "energy deposited by nonelastic interactions" were obtained by subtracting the energy which is given to cascade and evaporation neutrons and cascade protons from the energy removed from the incident beam, since these particles can migrate some distance away from the point of nonelastic interaction. Assuming that the energy of all the remaining particles created in the nonelastic event is sufficiently low to be deposited locally, then the four solid lines in Fig. 17 should fairly accurately depict the energy deposited by nonelastic interactions. As will be observed, these curves tend to cross each other

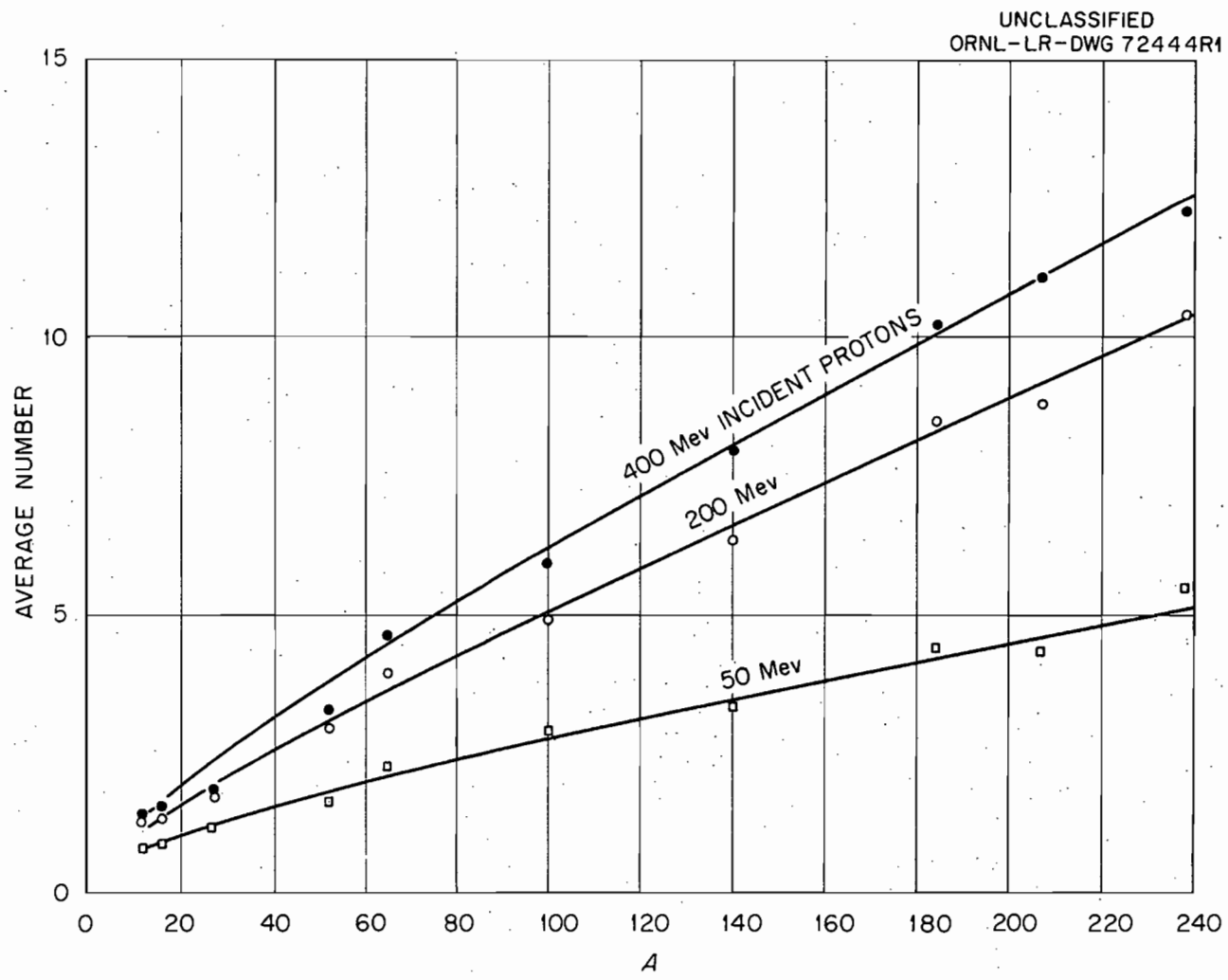

Fig. 15. Average Number of Cascade and Evaporation Neutrons vs. Atomic Mass Number A per Nonelastic Proton Event.

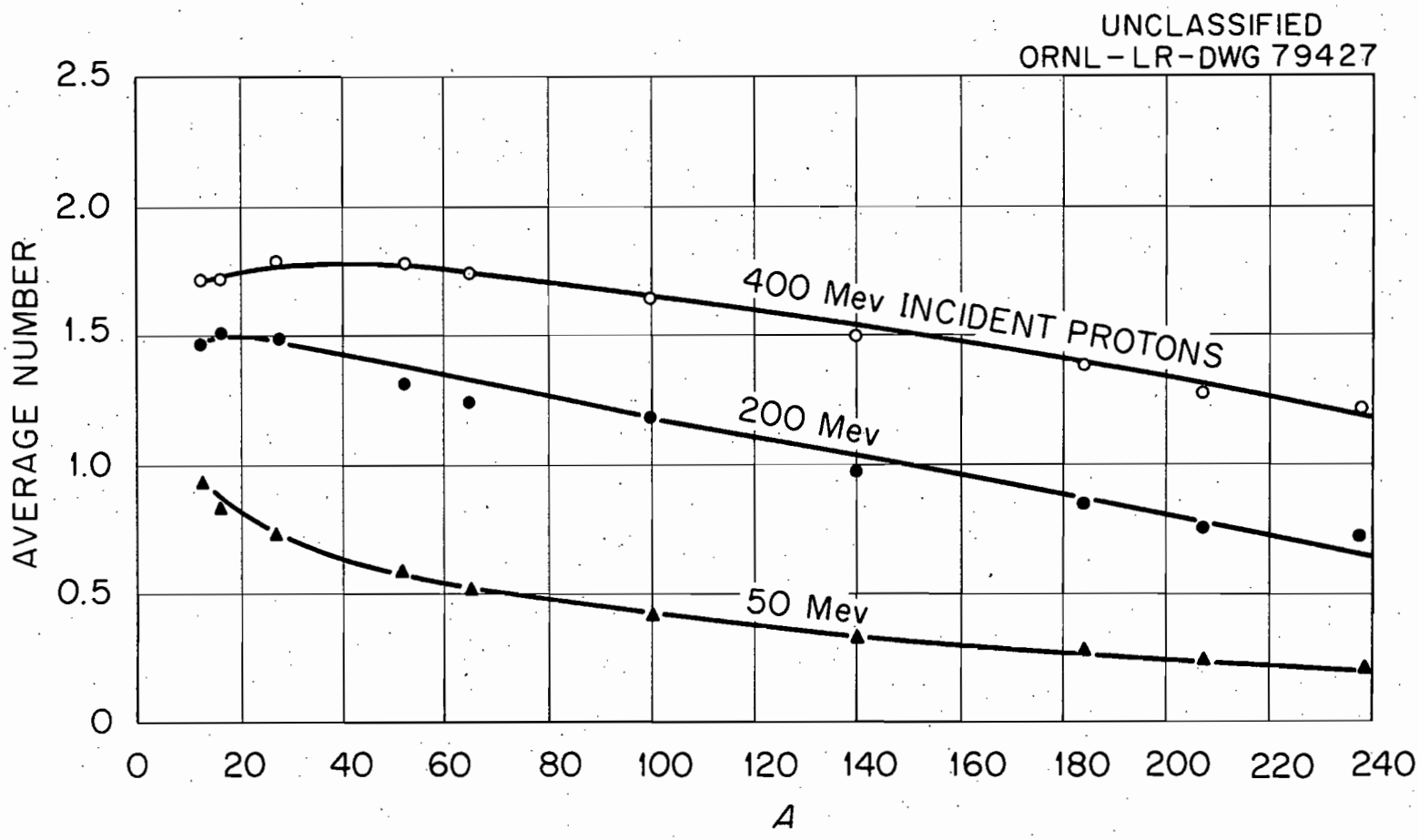

Fig. 16. Average Number of Cascade Protons vs. Atomic Mass Number A per Nonelastic Proton Event.

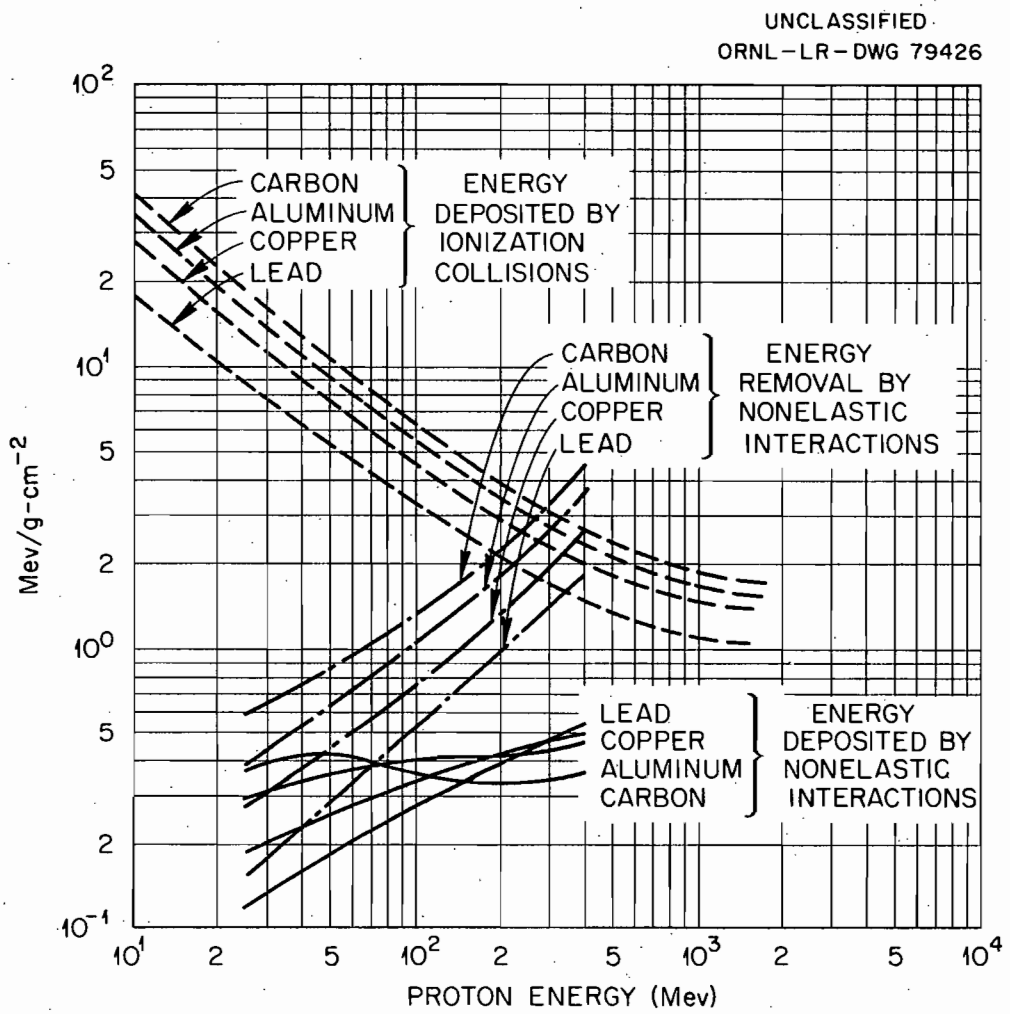

Fig. 17. Energy Removal and Deposition by Proton Beams.

at energies above 100 MeV, indicating that the heavy-atomic-weight materials might yield the lightest-weight shields for high-energy particles. For energies up to 400 MeV, however, the energy deposited by ionization collisions dominates the attenuation problem, and the lightest-atomic-weight materials still remain the best materials for shielding against protons.

The relative importance of secondary radiation produced by proton interactions to the overall penetration problem is indicated in Fig. 18 for the case of an aluminum shield.[9] In this case it is assumed that a 400-MeV proton beam is incident on the shield. Not all components of the secondary radiation are included in the figure, but in all cases shown the contribution to the penetrating dose rate is lower, by a factor of approximately 10, than the dose rate created by the penetrating primary particles for depths shorter than the range of the primary particle. For depths in the shield greater than the range of the primary particle, the secondary particles dominate the penetration problem.

For thin shields such as those that might be used on space vehicles in exploration of space close to earth, secondary particles can be expected to contribute only a small percentage of the penetrating radiation. But this must not be construed to mean that the secondary radiations can be neglected in all cases, because there are actually two distinct problems: one resulting from the secondary radiations created in the structural and shielding materials of the vehicle, and the other resulting from the secondary radiation produced in the astronaut.

The effect of secondary particles on the energy deposition as a function of depth in tissue is shown in Fig. 19.[10] Although the recoil nuclei and evaporation charged particles contribute only a rather small percentage to the energy deposition, it is exactly these particles that usually cause the greatest biological damage. Therefore the energy deposition by these particles is usually multiplied by a factor of 10

---

9. Neutron Phys. Div. Space Radiation Shielding Research Ann. Prog. Rep. Aug. 31, 1962, ORNL-CF-62-10-29 (Rev.) (1962), Paper I-4, Fig. 4.
10. Op. cit. Fig. 1, p. 119.

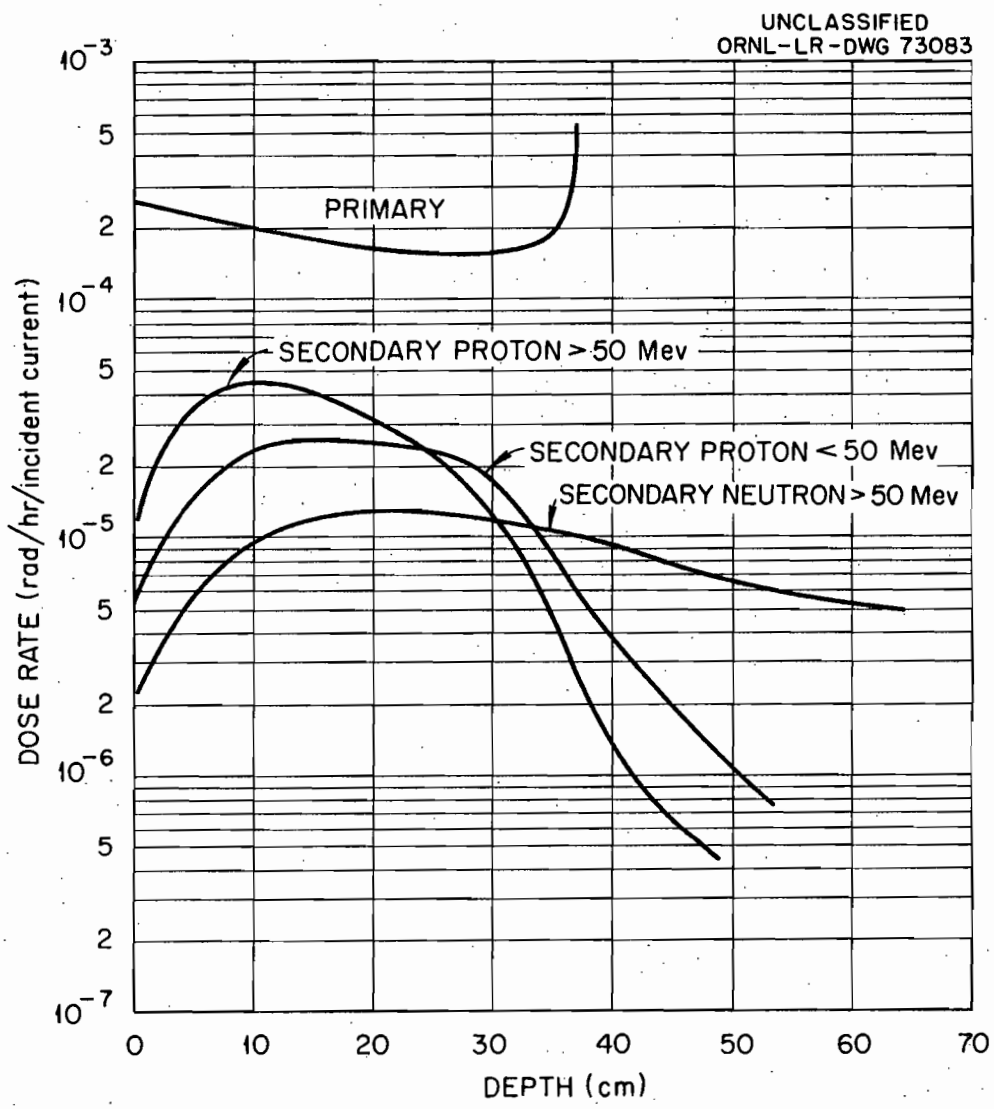

Fig. 18. Partial Dose Rates as a Function of Depth in 65-cm-thick Aluminum Slab from Normally Incident 400-MeV Protons.

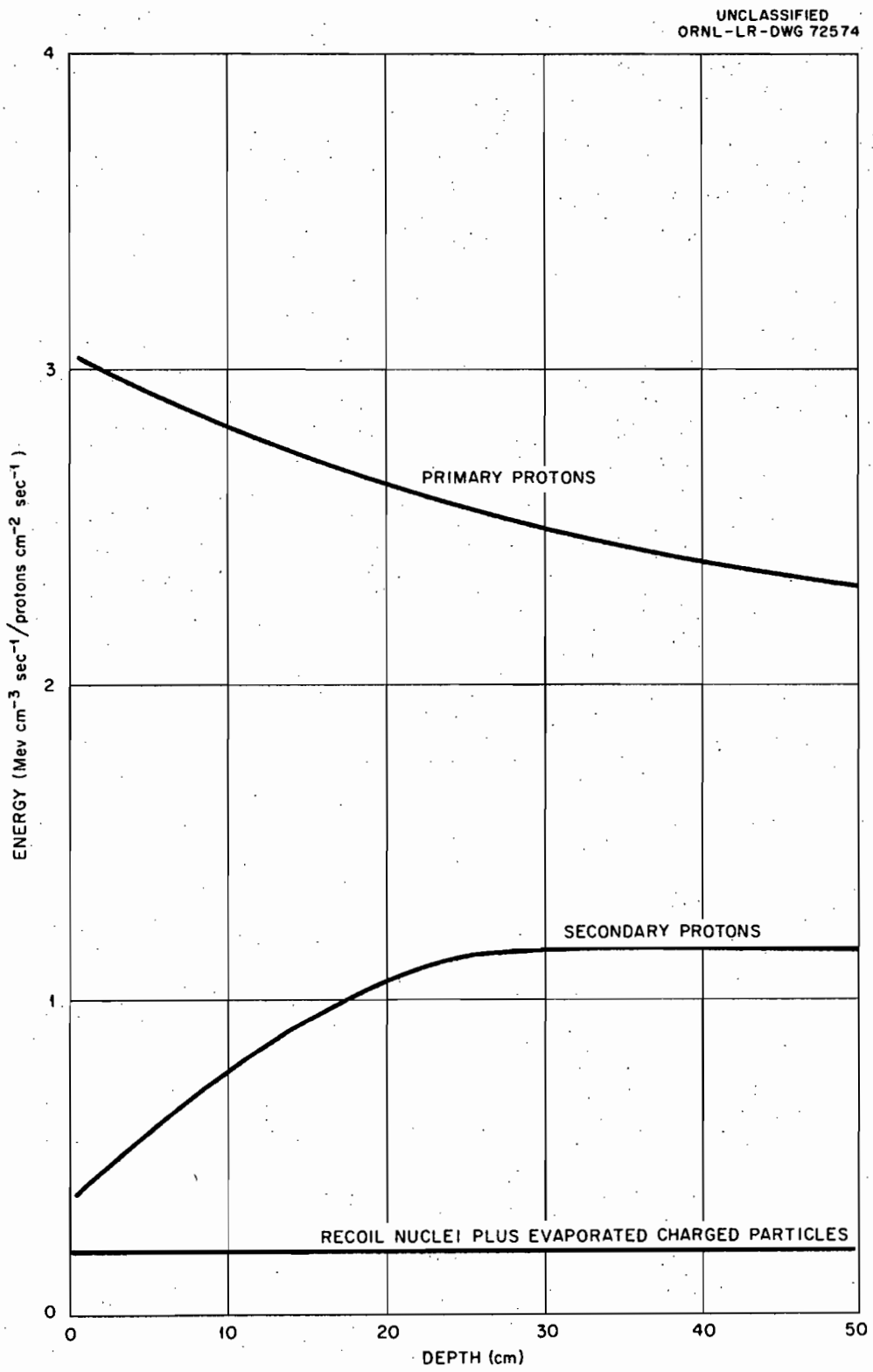

Fig. 19. Energy Deposition Resulting from 400-MeV Protons Normally Incident on a 50-cm-thick Infinite Slab of Tissue as a Function of Depth of Penetration.

to 20 to account for their enhanced biologically damaging effect. In such cases, the dose rate from these recoil nuclei and evaporation charged particles would be comparable to that from the primary protons. Consequently, if the shield is thin, the secondary particles created therein may not play a significant part in the penetration problem, but those produced in the body may contribute a large biological dose to the astronaut.

In summary it can be stated that light atomic weight materials will generally provide the lightest weight shields for the type of radiations encountered in space. This is generally true provided secondary electromagnetic radiation does not dominate the attenuation problem, in which case a combination of light atomic weight material followed by a heavy atomic weight material may provide the lightest weight shields.

Appendix A

The following tables were prepared from the data calculated by H. W. Bertini and L. Dresner[7] and are included here because of their general usefulness.

Page No.

Table A.1. Total Nonelastic Cross Sections for Protons Incident on Various Targets at Energies of 25 to 400 MeV 32

Table A.2. Average Number of Cascade Neutrons Emitted per Nonelastic Proton Interaction with Various Targets at Energies of 25 to 400 MeV 33

Table A.3. Average Energy of Cascade Neutrons Resulting from Nonelastic Proton Interaction with Various Targets at Energies of 25 to 400 MeV 34

Table A.4. Average Number of Cascade Protons Emitted per Nonelastic Proton Interaction with Various Targets at Energies of 25 to 400 MeV 35

Table A.5. Average Energy of Cascade Protons Resulting from Nonelastic Proton Interaction with Various Targets at Energies of 25 to 400 MeV 36

Table A.6. Average Number of Evaporation Neutrons Emitted per Nonelastic Proton Interaction with Various Targets at Energies of 25 to 400 MeV 37

Table A.7. Average Energy of Evaporation Neutrons Resulting from Nonelastic Proton Interaction with Various Targets at Energies of 25 to 400 MeV 38

Table A.1. Total Nonelastic Cross Sections for Protons Incident on Various Targets at Energies of 25 to 400 MeV

	Cross Section (mb)				
	Incident Proton Energy				
Target	25 MeV	50 MeV	100 MeV	200 MeV	400 MeV
$_{6}C^{12}$	454	356	257	225	227
$_{8}O^{16}$	524	407	316	283	281
$_{13}Al^{27}$	698	587	479	402	420
$_{24}Cr^{52}$	1007	857	728	655	659
$_{29}Cu^{65}$	1143	988	832	763	735
$_{44}Ru^{100}$	1434	1242	1101	1006	1019
$_{58}Ce^{140}$	1715	1556	1361	1250	1234
$_{74}W^{184}$	2018	1790	1620	1448	1458
$_{82}Pb^{207}$	2160	1928	1738	1663	1618
$_{92}U^{238}$	2323	2111	1918	1746	1770

Table A.2. Average Number of Cascade Neutrons Emitted per Nonelastic Proton Interaction with Various Targets at Energies of 25 to 400 MeV

	Number of Cascade Neutrons Emitted per Nonelastic Proton Interaction				
	Incident Proton Energy				
Target	25 MeV	50 MeV	100 MeV	200 MeV	400 MeV
$_{6}C^{12}$	0.45	0.64	0.88	0.93	0.95
$_{8}O^{16}$	0.41	0.61	0.87	0.94	1.030
$_{13}Al^{27}$	0.34	0.62	0.88	1.09	1.23
$_{24}Cr^{52}$	0.27	0.50	0.83	1.21	1.43
$_{29}Cu^{65}$	0.26	0.48	0.83	1.21	1.55
$_{44}Ru^{100}$	0.20	0.41	0.76	1.14	1.70
$_{58}Ce^{140}$	0.17	0.37	0.71	1.17	1.73
$_{74}W^{184}$	0.13	0.31	0.65	1.07	1.70
$_{82}Pb^{207}$	0.12	0.30	0.63	1.12	1.73
$_{92}U^{238}$	0.11	0.27	0.57	1.10	1.66

Table A.3. Average Energy of Cascade Neutrons Resulting from Nonelastic Proton Interaction with Various Targets at Energies of 25 to 400 MeV

	Average Cascade Neutron Energy (MeV)				
	Incident Proton Energy				
Target	25 MeV	50 MeV	100 MeV	200 MeV	400 MeV
$_{6}C^{12}$	8.6	14.7	31.3	67.5	120.8
$_{8}O^{16}$	8.2	15.3	29.1	60.0	105.8
$_{13}Al^{27}$	9.1	14.8	29.3	53.6	98.1
$_{24}Cr^{52}$	9.4	14.8	28.0	48.8	85.8
$_{29}Cu^{65}$	9.4	15.6	26.7	47.6	85.0
$_{44}Ru^{100}$	10.4	17.0	27.3	45.4	74.6
$_{58}Ce^{140}$	11.7	17.1	27.7	46.3	74.8
$_{74}W^{184}$	12.3	17.8	29.2	45.2	72.3
$_{82}Pb^{207}$	12.2	18.7	28.7	49.3	70.5
$_{92}U^{238}$	12.3	19.7	31.0	45.6	67.9

Table A.4. Average Number of Cascade Protons Emitted per Nonelastic Proton Interaction with Various Targets at Energies of 25 to 400 MeV

	Number of Cascade Protons Emitted per Nonelastic Proton Interaction				
	Incident Proton Energy				
Target	25 MeV	50 MeV	100 MeV	200 MeV	400 MeV
$_{6}C^{12}$	0.57	0.92	1.24	1.47	1.72
$_{8}O^{16}$	0.53	0.83	1.19	1.52	1.72
$_{13}Al^{27}$	0.45	0.73	1.12	1.50	1.79
$_{24}Cr^{52}$	0.32	0.60	0.91	1.31	1.79
$_{29}Cu^{65}$	0.30	0.52	0.84	1.24	1.74
$_{44}Ru^{100}$	0.20	0.41	0.71	1.19	1.64
$_{58}Ce^{140}$	0.14	0.32	9.57	0.97	1.51
$_{74}W^{184}$	0.11	0.28	0.49	0.85	1.39
$_{82}Pb^{207}$	0.10	0.24	0.46	0.75	1.28
$_{92}U^{238}$	0.08	0.21	0.41	0.72	1.24

Table A.5. Average Energy of Cascade Protons Resulting from Nonelastic Proton Interaction with Various Targets at Energies of 25 to 400 MeV

	Average Cascade Proton Energy (MeV)				
	Incident Proton Energy				
Target	25 MeV	50 MeV	100 MeV	200 MeV	400 MeV
$_{6}C^{12}$	8.8	17.3	34.6	72.1	146.5
$_{8}O^{16}$	8.8	18.6	34.5	70.6	147.2
$_{13}Al^{27}$	9.1	17.0	30.9	62.3	127.5
$_{24}Cr^{52}$	9.3	16.8	31.4	59.4	114.2
$_{29}Cu^{65}$	9.5	17.8	31.0	59.3	104.4
$_{44}Ru^{100}$	10.7	18.0	29.8	56.1	99.7
$_{58}Ce^{140}$	11.1	19.1	31.9	56.6	96.8
$_{74}W^{184}$	11.9	19.1	32.5	61.6	100.4
$_{82}Pb^{207}$	12.4	20.0	33.9	60.0	101.1
$_{92}U^{238}$	13.2	20.7	33.5	57.1	105.7

Table A.6. Average Number of Evaporation Neutrons Emitted per Nonelastic Proton Interaction with Various Targets at Energies of 25 to 400 MeV

	Number of Evaporation Neutrons Emitted per Nonelastic Proton Interaction				
	Incident Proton Energy				
Target	25 MeV	50 MeV	100 MeV	200 MeV	400 MeV
$_{6}C^{12}$	0.04	0.19	0.28	0.35	0.41
$_{8}O^{16}$	0.07	0.26	0.39	0.39	0.48
$_{13}Al^{27}$	0.37	0.54	0.59	0.60	0.61
$_{24}Cr^{52}$	0.74	1.12	1.45	1.76	1.92
$_{29}Cu^{65}$	1.18	1.78	2.40	2.69	3.11
$_{44}Ru^{100}$	1.73	2.46	3.22	3.73	4.22
$_{58}Ce^{140}$	2.24	3.01	4.23	5.22	6.25
$_{74}W^{184}$	2.57	4.11	5.95	7.70	9.08
$_{82}Pb^{207}$	2.56	4.06	6.02	8.11	10.62
$_{92}U^{238}$	3.47	5.23	7.71	10.67	13.18

Table A.7. Average Energy of Evaporation Neutrons Resulting from Nonelastic Proton Interaction with Various Targets at Energies of 25 to 400 MeV

	Average Evaporation Neutron Energy (MeV)				
	Incident Proton Energy				
Target	25 MeV	50 MeV	100 MeV	200 MeV	400 MeV
$_{6}C^{12}$	3.6	4.7	5.7	6.1	5.5
$_{8}O^{16}$	3.2	3.6	5.0	5.6	5.5
$_{13}Al^{27}$	1.5	2.9	4.0	4.7	4.7
$_{24}Cr^{52}$	2.0	2.6	3.7	3.7	4.2
$_{29}Cu^{65}$	1.8	2.3	3.0	3.7	4.1
$_{44}Ru^{100}$	1.6	2.1	2.7	3.2	3.8
$_{58}Ce^{140}$	1.3	1.9	2.4	2.9	3.5
$_{74}W^{184}$	1.3	1.7	2.2	2.7	3.2
$_{82}Pb^{207}$	1.3	1.6	2.1	2.6	3.2
$_{92}U^{238}$	1.2	1.5	2.0	2.5	3.1

Internal Distribution

1. F. S. Alsmiller
2. R. G. Alsmiller, Jr.
3. H. W. Bertini
4. E. P. Blizard
5. T. V. Blosser
6. W. R. Burrus
7. R. R. Coveyou
8. R. L. Cowperthwaite
9. L. E. Cruse
10. W. A. Gibson
11. W. H. Jordan
12. W. E. Kinney
13. C. F. Johnson
14. T. A. Love
15. F. C. Maienschein
16. H. S. Moran
17. R. W. Peelle
18. R. T. Santoro
19-28. C. D. Zerby
29. W. Zobel
30-31. Central Research Library
32. Document Reference Section
33-52. Laboratory Records
53. Laboratory Records ORNL, R.C.
54-68. Division of Technical Information Extension (DTIE)
69. Research and Development Division (ORO)

External Distribution

70-71. O. L. Tiffany and Keith More; Bendix Systems Division, Ann Arbor, Michigan
72. Herman J. Schaefer; U.S. Naval School of Aviation, Pensacola, Fla.
73-74. E. C. Smith and W. M. Schofield; Advance Research Corp. Lafayette, Indiana
75-76. J. W. Keller and Lt. Col. Joseph Conner; NASA, Washington, D.C.
77. E. O. Berdahl; Scientific Advisor, TDX1A, Wright-Patterson Air Force Base, Ohio
78-83. Capt. R. F. Cooper, C. A. Dempsey, Maj. James F. Dinwiddie, T. J. McGuire, L. Pittman, and J. Speakman; WADC, Dayton, Ohio
84. H. Schulte; Bellcomm, Inc., Washington, D.C.
85. R. V. Glowczwski; McDonnell Aircraft, St. Louis, Missouri
86. R. A. Glass; Lockheed Missiles and Space Company, Dept. 52-10, Palo Alto, California
87. G. A. Whan; The University of New Mexico, Albuquerque, New Mexico
88. K. D. George; Reactor Requirements Office, Picatinny Arsenal, Dover, New Jersey
89. F. L. Keller; Aerospace Corporation, El Segundo, California
90. D. H. Robey; General Dynamics/Astronautics, San Diego, Calif.
91. W. H. Langham; Los Alamos Scientific Laboratory, Los Alamos, New Mexico
92-95. L. F. Vosteen, W. C. Hulton, T. Foelsche, and J. E. Duberg; NASA, Langley Field, Virginia
96. D. Langford; Pratt and Whitney Aircraft, East Hartford, Conn.
97-100. R. H. Steelle, C. Warren, W. L. Gill, and L. N. McMillion; NASA, Manned Space Craft Center, Houston, Texas
101-102. R. Shelton and H. E. Stern; NASA, Huntsville, Alabama
103-106. K. R. Pinckney, G. E. Laubach, L. Clark, and M. R. Kinsler; North American Aviation, Downey, California
107. E. R. Beever; Space and Information Systems Division, North American Aviation, Inc., Downey, California

108. J. P. T. Pearman; National Academy of Sciences, Washington, D.C.
109. D. W. Drawbaugh; Westinghouse Electric Company, Pittsburgh, Pa.
110-111. Lt. Col. Ralph G. Allen, Jr. and Col. John E. Pickering; USAF Aerospace Medical Center, Brooks Air Force Base, Texas
112. Charles Hill; Lockheed Aircraft, Marietta, Georgia
113. E. M. Finkelman; Grummon Aircraft, Bethpage, New York
114. P. Mittleman; United Nuclear Corp., White Plains, New York
115. Ray Aronson; Technical Research Group, Syossett, New York
116. R. Madey; Republic Aviation Corp., Farmingdale, Long Island, New York
117-118. I. M. Karp and R. I. Hildebrand; Lewis Research Center, Cleveland, Ohio
119-121. D. L. Dye, M. Pearson, and J. C. Noyes; Boeing Aircraft Co., Seattle, Washington
122-123. R. V. Meghreblian and D. F. Spencer; Jet Propulsion Laboratory, Pasadena, California
124-128. R. Wallace, W. Patterson, C. Sondhaus, C. Tobias, and B. J. Moyer; University of California, Berkeley, California
129. R. B. Curtis; University of Indiana, Bloomington, Indiana
130. S. P. Shen; New York University, New York, New York
131. L. Jackson Laslett; Chief, High-Energy Physics Branch, U.S. Atomic Energy Commission Division of Research, Washington, D.C.
132-133. F. McDonald and W. N. Hess; Goddard Space Flight Center, Greenbelt, Maryland
134-138. R. French, N. Schaeffer, T. W. Deveries, T. J. Rock, and S. Dominey; General Dynamics, Fort Worth, Texas
139. M. J. Berger; National Bureau of Standards, Washington, D.C.
140. J. P. Neissel; General Engineering Laboratory, General Electric Company, Schenectady, New York
141. S. Krasner; Office of Naval Research, Washington 25, D.C.
142. E. V. Vaughan; Atomics International, Canoga Park, California
143-145. S. Russak, A. J. Beck, and E. Divita; The Martin Company, Baltimore, Maryland
146-148. M. C. Chapman, R. E. Fortney, and S. H. Levine; Northrup Space Laboratory, Los Angeles, California
149. W. Steigelmann; Franklin Institute, Philadelphia, Pa.
150. Capt. W. A. Anders; USAF, AFSWC (SWVPF), Kirtland AFB, New Mexico
151. Martin Leimdorfer; Head, Theoretical Shielding Group, Aktiebolaget Atomenenergi, Reactor Development Division, Stockholm 0, Sweden